FLOW PATTERN AND EXPERIMENTAL INVESTIGATION OF HEAT TRANSFER COEFFICIENTS DURING THE CONDENSATION OF R134A AT LOW MASS FLUXES IN A SMOOTH HORIZONTAL TUBE

Ewim D.R.E., Kombo R. and Meyer, J.P*.
Department of Mechanical and Aeronautical Engineering,
University of Pretoria,
Pretoria, 0002,
South Africa,
E-mail: josua.meyer@up.ac.za

ABSTRACT

An experimental study of heat transfer and flow pattern visualisation during the condensation of R134a was conducted in a smooth horizontal tube at low mass fluxes. Most previous experimental and analytical studies on in-tube condensation were conducted at high mass fluxes. In these studies, it was found that the heat transfer coefficient was not a function of the temperature difference between the tube wall temperature and condensation temperature. In addition, most heat transfer models developed were for high mass fluxes and failed to predict heat transfer coefficients at low mass fluxes properly. However, the most recent predictive heat transfer models have been based on studying and analysing the flow patterns. In all of these, only very few experimental studies have been coupled with flow pattern identification at different controlled temperature differences and mean vapour qualities at low mass fluxes. Therefore, the purpose of this study was the investigation of R134a condensing at low mass fluxes (20 –100 kg/m²s) and the identification and analysis of the flow patterns observed. The experiments were conducted in a smooth horizontal tube 8.38 mm in internal diameter with a length of 1.5 m at different mean vapour qualities and controlled temperature differences. The average saturation temperature was maintained at 40°C. The flow patterns were recorded simultaneously with a high speed video camera at the inlet and outlet of the test section through transparent sight glasses. The results showed that stratified flow and stratified-wavy were the dominant flow patterns. Stratification would differ with decreasing flow rate of the refrigerant. As the flow rate decreased, the liquid layer at the bottom of the tube increased. The study also revealed the effect of temperature difference between the tube wall and the saturation temperatures with respect to the heat transfer coefficient at low mass flow rates of the refrigerant. The higher the temperature difference, the lower the heat transfer coefficient.

INTRODUCTION

The most common outcomes of heat transfer coefficient investigation for in-tube condensation have shown that the heat and momentum transfer processes are strongly influenced by the prevailing flow pattern [1]. Consequently, the latest heat transfer models that have been proposed have been flow pattern based [2-6]. However, Dobson and Chato [3] mentioned some disagreements of various authors in literature with regards to the differences in the predictions of flow patterns which are either controlled by gravity or shear forces.

Nevertheless, there is a general agreement with research findings [3, 9-11] that temperature difference is the driving mechanism for heat transfer at low mass velocities (gravity driven flows).

In all of these, the majority of research works have been at mass fluxes between 200 kg/m²s and higher (typically up to 1000 kg/m²s). The few research works at low mass fluxes have not been being coupled with flow patterns to properly characterize flows at low mass fluxes. In other cases, the effect of temperature difference has not been studied and quantified. This is in contrast with the assertion of Thome [7] that temperature difference is the driving mechanism for heat transfer at low mass velocities.

Aprea et al. [8] and Lee and Son [9] noted that heat transfer coefficients for gravity driven flows were enhanced at high vapour qualities and lower at low vapour qualities. They also found the dependency of heat transfer on vapour quality was stronger at high velocities of the fluid. However, they did not study the flow regimes and did not investigate the effect of temperature difference on the heat transfer coefficients. Dobson and Chato [3] observed in their experimental study that for low mass velocities, the flow pattern was not affected by changes in the nature of refrigerant or tube diameter. They noted that shear controlled flows were due to the high vapour flow velocities. They also noted a significant impact on the heat transfer rate due to temperature difference for gravity driven flow. An increase in temperature difference led to a decrease in the Nusselt numbers for the whole range of vapour quality.

Various flow pattern maps have been developed previously to predict transition of flow patterns for diabatic and adiabatic conditions [1, 6, 10, 11]. The first proposed two-phase flow pattern map for boiling in horizontal tubes was by Kattan et al. [1]. The flow pattern model and map showed an improvement in the prediction of heat transfer when compared to other previous methods. El-Hajal et. al [10] developed condensing flow pattern map in a horizontal tube, a development of the Steiner flow [12] pattern map. Soliman flow pattern map [13-15] did not have the stratified and stratified wavy region but instead used wavy flow to predict low mass fluxes. Dobson and Chato's [3] low velocity data fell on the wavy flow region on the Soliman flow map although the observed flow pattern was stratified and stratified wavy flow.

It can therefore be concluded from previous studies that there is a need to carry out better quantitative studies at low mass fluxes.

It can also be deduced that very few comprehensive studies on gravity dominated flows from as low as 25 kg/m²s to about 200 kg/m²s specifically to determine the heat transfer coefficients and capture the flow regime as function of controlled temperature difference between the test section wall saturation temperature and condensing temperature has been carried out. Therefore, it is the purpose of this study to experimentally determine the heat transfer coefficients and present new reliable, consistent and repeatable data in a smooth horizontal tube at low mass fluxes at different mean vapour qualities and temperature differences (ΔT) between the test section wall temperature and condensing temperature. The flow regime will also be captured and analysed.

NOMENCLATURE

A	[m²]	Surface area
C_p	[J/kgK]	Specific heat
d	[m]	Diameter
EB	[%]	Energy balance
g	[m²s]	Gravitational acceleration
G	[kg/m²s]	Specific enthalpy
k	[W/mK]	Thermal conductivity
L	[m]	Length of test section
$\dot{m}$	[kg/s]	Mass flow rate
ΔP	[Pa]	Pressure drop
Q	[W]	Heat transfer rate
R	[K/W]	Thermal resistance
T	[ºC]	Temperature
x	[-]	Vapour quality
z	[-]	Axial direction

Special characters
α	[W/m²K]	Heat transfer coefficient

Subscripts
CS	Cross-Section
Cu	Copper
H_2O	Water
i	Inner
in	Inlet
j	Measurement location
l	Liquid
o	Outer
out	Outlet
$post$	Post-condenser
pre	Pre-condenser
ref	Refrigerant
sat	Saturation
$test$	Test-condenser
tot	Total
v	Vapour
w	Water, wall

EXPERIMENTAL APPARATUS AND PROCEDURE

The test bench used for this investigation has been used previously for several research projects on condensation but was modified to accommodate the special needs of this study. The experimental test rig was made of two distinct cycles: namely a vapour compression refrigerant cycle (red lines) and a water cycle (blue lines) as shown schematically in Figure 1. The vapour compression cycle was made up of the test section line and the bypass line which are high pressure lines and a low pressure line through which the R134a was pumped using a hermetic scroll compressor with a nominal capacity of 10 kW. Each of the lines had two electronic expansion valves (EEVs) which controlled the mass flow rate of the refrigerant. The test line had three condensers: the pre-condenser, the test condenser containing the test section and the post-condenser. The pre condenser was used to control the inlet vapour quality (x) into the test section where the actual measurements and experiments were carried out and the post-condenser was used to ensure that complete condensation and sub cooling occurred to ensure that the refrigerant mass flow rate could be measured correctly. The bypass line had a bypass condenser that controlled the pressure, temperature and mass flow rate of the refrigerant flowing into and through the test line; the majority of the refrigerant flowed through the bypass line and only a small fraction flowed through the test section line. The refrigerant from the high pressure lines was throttled in the EEVs into the low pressure line consisting of a water heated evaporator, suction accumulator and a scroll compressor.

The water that was used for the condensation and evaporation was stored and supplied from three insulated water tanks. Two of the three tanks were storage tanks with capacities of 500 litres each. These tanks were kept at pre-selected temperatures and thermostatically controlled between 15°C and 40°C. The colder temperature line was used in all the condensers and the warmer temperature line was used for the water heated evaporator. The third tank was part of a thermal bath from which water was supplied to annulus of the test section. This bath allowed for adequate temperature and water flow control to attain the desired temperature difference and was operated with water inlet temperature varying from 10°C to 20°C depending on the desired refrigerant mass flux, temperature difference and vapour quality. The test section was a smooth copper in-tube heat exchanger wherein the refrigerant flowed in the inner tube and water flowed in a counter flow direction through the annulus. The test section inner tube was 1.5 m in length with an inner diameter of 8.38 mm while the outer tube through which the cooling water flowed had an inner diameter of 14.5 mm. To guarantee that the flow through the test condenser was fully developed, a straight calming section, 500 mm long was positioned at the entrance to the test section (after the sight glasses) and another calming section, 400 mm long was positioned at the exit of the test condenser to minimise the disturbance at the exit sight glass. The purpose of the sight glasses was to enable flow visualisation and capture videos of the flow regimes. They also served as insulators against axial heat conduction. The flow regimes were captured with a high speed video camera (200 frames per second). A uniform backlight was installed against the sight glass to ensure uniformity in the distribution of the light emitting diode (LED) and this allowed for good colour fidelity.

On the outside surface of the test section tube, twenty-eight (28) shallow drilled holes were made at seven stations marked (A-G) equidistant to one another along the tube. The first station was at a distance of 70 mm from the inlet of the tube with a subsequent spacing of 225 mm after each position following on from the first. Each station had four shallow drilled holes at equal distances around the circumference of each position where the T-type thermocouples (copper-constantan) were used to

measure the outside tube wall temperature and were attached to the wall by soldering. All the thermocouples used were calibrated against a calibrated (PT100) to an accuracy of $\pm\,0.1^\circ$C. The refrigerant and water mass flow rates through the three condensers were measured with a Coriolis mass flow meter. The refrigerant pressure at the inlet to the test condenser was measured with a strain gauge pressure transducer to an accuracy of ± 2 kPa. In order to calculate the energy balance, water inlet and outlet temperatures in the pre and post condensers were measured. All measurements of temperatures, pressure and mass flux were taken at steady state conditions when no more fluctuations occurred, energy balance (EB) was less than 5% and constant for a period of 5 minutes. The readings from the Coriolis mass flow meters, pressure transducers and thermocouples were collected by a computerised data acquisition arrangement (DAQ) which comprised a desktop computer with LabVIEW. Also embedded in the DAQ were terminal blocks, channel multiplexers, termination units, transducer multiplexers, an interface card, and signal-conditioning extensions for instrumentation (SCXI). The readings were captured for 360 seconds (201 points) at the rate of 0.56 Hz and the averages of these values were used to calculate the fluid properties, heat transfer coefficient and other important parameters. The use of the average of the 201 points was to minimise experimental errors due to noise measurements. The standard deviations of the 201 points were monitored to check for stability. Table 1 presents the experimental variables and uncertainties.

Table 1: Experimental variables and uncertainties

Parameter	Range	Uncertainties
T_{sat}	40°C	$\pm 0.1^\circ$C
G	20-100 kg/m^{2}s	$\pm 5\%$
x_m	0.15-0.82	$\pm 5\%$
Q_{H2O}	50-400 W	$\pm 5\%$
α	1 200-2 500 W/m^{2}K	$\pm 13\%$

DATA REDUCTION

The experimental data points were taken at prescribed thermodynamic properties of the refrigerant. One of the key parameters that was useful in getting the desired point was the vapour quality (x). For the purpose of this study, we made use of the inlet (x_{in}), outlet (x_{out}) and mean vapour qualities (x_m). The refrigerant vapour quality at the inlet of the test condenser (x_{in}) was determined from the specific enthalpy of the refrigerant at the inlet to the pre-condenser and the specific enthalpies of the vapour and liquid states of the refrigerants (h_l and h_v) at the same temperature and pressure conditions.
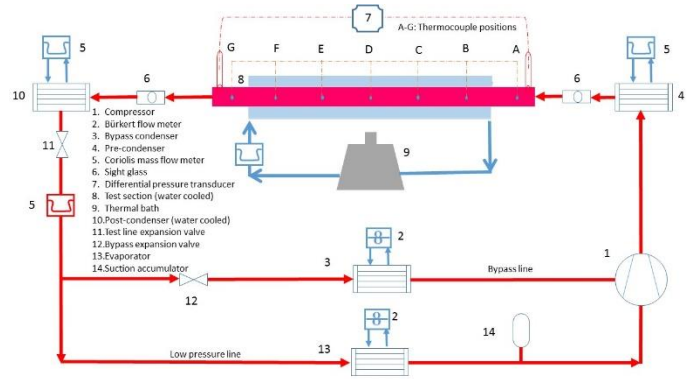

Figure 1. Schematic diagram of the experimental lay-out

To determine the refrigerant properties at the entrance of the pre-condenser and exit of the post- condenser, temperature and pressure measurements were utilized together with the thermodynamic properties of the condensing fluid (R134a). All of these were determined by the use of a refrigerant property data base REFPROP [16]. Mathematically, the vapour quality is written in Eq. 1 as:

$$x_{in} = \frac{h_{test,in} - h_l}{h_v - h_l} \tag{1}$$

The specific enthalpy of the refrigerant at the entrance of the test section $h_{test,in}$ was calculated from the specific enthalpy of the refrigerant at the inlet to the pre-condenser (acquired using the temperature and pressure conditions at the inlet to the pre-condenser), the calculated rate of heat transfer in the pre-condenser, $Q_{ref,pre}$ and the measured mass flow rate of the refrigerant, $\dot{m}_{ref}$ which was constant throughout the test-line. It is given in Eq. 2 as:

$$h_{test,in} = h_{pre,in} - \frac{|Q_{ref,pre}|}{\dot{m}_{ref}} \tag{2}$$

Here, $h_{pre,in}$ is the specific enthalpy of the refrigerant at superheated condition gotten from the by the use of a refrigerant property data base REFPROP [16]. Neglecting losses, the calculated rate of refrigerant heat transfer in the pre-condenser, $Q_{ref,pre}$ was equal to the water side rate of heat gain, $Q_{w,pre}$ and can be written in Eq. 3 as:

$$Q_{w,pre} \approx \dot{m}_{w,pre} C_p \left(T_{w,pre-out} - T_{w,pre-in} \right) \tag{3}$$

Here, $\dot{m}_{w,pre}$ is the measured water mass flow rate through the pre-condenser, C_p is the specific heat capacity of the water interpolated at the average cooling water temperature entering and leaving the pre-condenser, $T_{w,pre-out}$ is the measured water temperature (the mean of 3 thermocouples readings) at the exit of the pre-condenser, $T_{w,pre-in}$ is the measured water temperature (the mean of 3 thermocouples readings) at the entrance of the pre-condenser, The vapour quality of the refrigerant exiting the test condenser given in Eq. 4 also takes the form of Eq. 1 and is given by:

$$x_{out} = \frac{h_{test,out} - h_l}{h_v - h_l} \tag{4}$$

Here, the specific enthalpy of the refrigerant at the exit of the test section $h_{test,out}$ was determined from the enthalpy of the refrigerant at the inlet to the test section (already derived above in Eq. 2), the rate of heat transfer in the test condenser, $Q_{ref,test}$ and the measured mass flow rate of the refrigerant, $\dot{m}_{ref}$ which was constant throughout the test-line is given as:

$$h_{test,out} = h_{test,in} - \frac{|Q_{ref,test}|}{\dot{m}_{ref}} \tag{5}$$

Neglecting losses, the calculated rate of heat transfer in the test-condenser, $Q_{ref,test}$ was equal to the water side rate of heat gain, $Q_{w,test}$ and can be written as:

$$Q_{w,test} \approx \dot{m}_{w,test} C_p (T_{w,test-out} - T_{w,test-in}) \tag{6}$$

The data points were taken at various mean vapour qualities and were calculated as shown in Eq. 7:

$$x_m = \frac{x_{out} + x_{in}}{2} \tag{7}$$

When the energy balance was less than 5%, it was right to assume that the heat transfer through the water side of the test section (i.e. the annulus), was equal to that of the refrigerant. Thus combining the water-side heat transfer information, together with the measured refrigerant mass flow, measured inlet and outlet temperatures, as well as the measured annulus-outer wall temperatures, it was possible to calculate the inner heat transfer coefficient. With Newton's law of cooling, the coefficient of heat transfer through the test condenser could be calculated using Eq. 8.

$$\alpha = \left| \frac{Q_{w,test}}{A(\overline{T}_{w,i} - T_{sat})} \right| \tag{8}$$

Here, $Q_{w,test}$ is the calculated water heat transfer rate across the test section and has already been given in Eq. 6., $\dot{m}_{w,test}$ is the measured water mass flow rate through the test section, C_p is the specific heat capacity of cooling the water through the test section interpolated at the average cooling water temperature, $T_{w,test-out}$ is the measured water temperature at the exit of the test section, $T_{w,test-in}$ is the measured water temperature at the entrance of the test section, A is the calculated inner surface area of the inner tube of the test section . T_{sat} is the measured mean saturation temperature between the inlet and outlet of the test section. $\overline{T}_{w,i}$ is the calculated mean inner wall temperature and it is related to the measured mean outer-wall temperature $\overline{T}_{w,o}$ of the tube through the thermal resistance of the wall of the copper tube R_w [K/W] as shown in Eq. 9 and 10

$$\overline{T}_{w,i} = \overline{T}_{w,o} + |Q_{test} R_w| \tag{9}$$

Here R_w is gotten from Fourier's law of heat conduction and is shown in Eq. 13.

$$R_w = \frac{\ln(d_o/d_i)}{2\pi k_{cu} L} \tag{10}$$

Here, d_o and d_i are the measured outer and inner diameters of the inner tube of the test section, L is the measured length of the test section and k_{cu} is the thermal conductivity of the copper tube gotten from literature. The average outer-wall temperature, $\overline{T}_{w,o}$ was calculated using the physical distance between stations and the trapezoidal numerical integration. It is shown in Eq. 11 as:

$$\overline{T}_{w,o} = \frac{1}{L} \sum_{j=1}^{7} [(T_{w,o}^j + T_{w,o}^{j+1})(z_{j+1} - z_j)] \tag{11}$$

Finally, the system energy balance was calculated to make sure that, all the assumptions made in the previous section were valid and no stray energy was lost in the system. The system energy balance Eq. 12 consisted of comparing the total test-line energy transferred inside the pre-, test- and post-condensers between the water and refrigerant lines.

$$EB = \frac{|Q_{ref,tot} - Q_{w,tot}|}{Q_{ref,tot}} \tag{12}$$

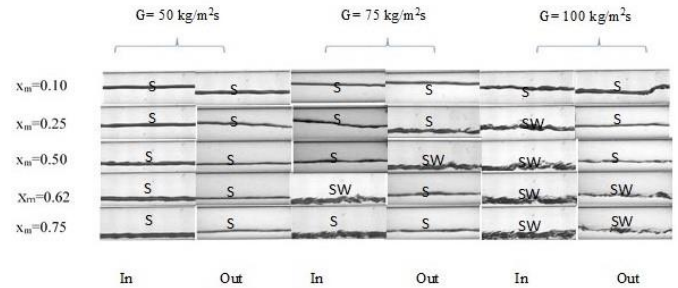## RESULTS AND DISCUSSION

Figure 2. Flow regime recognition at different mass fluxes

Fig. 2 shows the flow pattern visualized as function of both mass flux and mean vapour quality. It can be seen that the flow regimes were either stratified or stratified wavy. Due to finite difference in density between the liquid and vapour phases, the liquid phase moved along the bottom of the tube while the vapour phase moved on the top part. Furthermore, as the vapour quality increased, the density and gravity effect became significant as liquid condensate forming at the perimeter of the tube at a mean vapour quality of 0.15 was forced down to the bottom of the tube. At this low quality, the interface was maintained smooth due to the effect of gravity. However, at mean vapour quality of 0.75, there was a noticeable movement of the liquid phase down to the bottom perimeter of the tube as a result of gravity forces with the vapour taking over a substantial part of top of the tube and wave formation occurred. These waves developed at the liquid vapour interface through a Kelvin-Helmholtz Instability Mechanism and acted upon the vapour as a form of interfacial roughness. The wavy nature of the stratified flow could also be seen to increase with vapour quality. Consequently, the interfacial stress became larger than over a smooth and flat plane surface. That interfacial friction depended

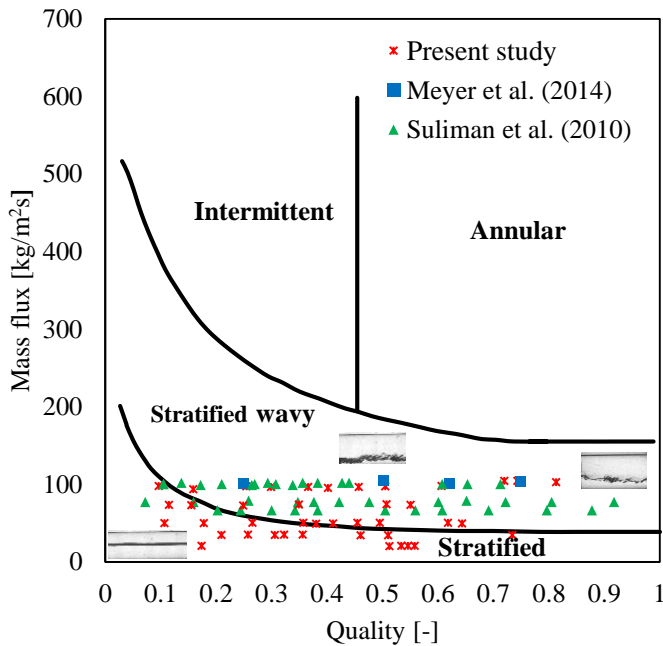on interfacial roughness, and the roughness itself depended on velocities of the phases.

Figure 3: Present data plotted on El Hajal Thome [10] map

In Fig.3, the experimental data was overlaid on the El Hajal-Thome-Cavallini [10] flow pattern map which was developed to predict flow patterns during condensation inside smooth horizontal tubes for different working fluids including R-134a. The flow pattern map had previously been used by Lips and Meyer [17-20], Suliman and Meyer [21, 22] and Meyer et al. [23] to predict their data. The map predicted the flow patterns showing stratified-wavy as the main dominant flow pattern for mass fluxes between 75 and 100 kg/m^{2}s. However, fully stratified flow was the only observed flow pattern for very low mass velocities of 35 kg/m^{2}s and less for all vapour qualities. However for very low qualities of below 0.25, stratified flow was the only pattern observed for all the mass velocities used for this study. Meyer et al. [23] and Suliman et al. [22] also had the same observations for the mass velocity of 100 kg/m^{2}s.

The effect of temperature difference on the heat transfer coefficients is shown in Fig. 4. The figure depicts heat transfer coefficients at a mass flux of 100 kg/m^{2}s plotted against the mean vapour qualities with respect to the four different temperature differences. It can be seen from this figure that the maximum heat transfer coefficients were found at the lowest (ΔT) of 3°C and were at the lowest (ΔT) of 10°C. It can be deduced that if we lowered the temperature difference below 3°C that the heat transfer coefficient was going to increase.
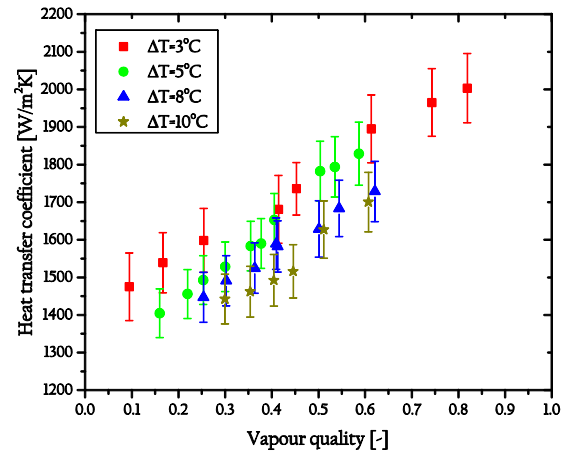

Figure 4. Effect of temperature difference on heat transfer coefficient (G=100 kg/m^{2}s, Horizontal flow)

However the experimental uncertainties would increase as found during the uncertainty analysis. The other temperature differences (5°C and 8° C) lay in between the data points. The temperature difference phenomenon influencing the heat transfer coefficient was not observed during the validation at mass fluxes higher than 200kg/m^{2}s. It can also be seen that the heat transfer coefficient increased as the mean vapour quality increased. However, this trend became less noticeable as the mass flux was lowered. This also became less noticeable as the temperature difference increased. For the same mass flux of 100 kg/m^{2}s, the local heat transfer coefficients decreased with an increase in temperature difference. This decrease occurred even though the heat transfer rate were higher to attain the higher temperature difference. This is in agreement with the findings of Arslan and Eskin [17] who however concentrated on a smooth vertical tube. The heat transfer coefficient also increased with mean vapour quality but was more dependent on the temperature difference (ΔT).
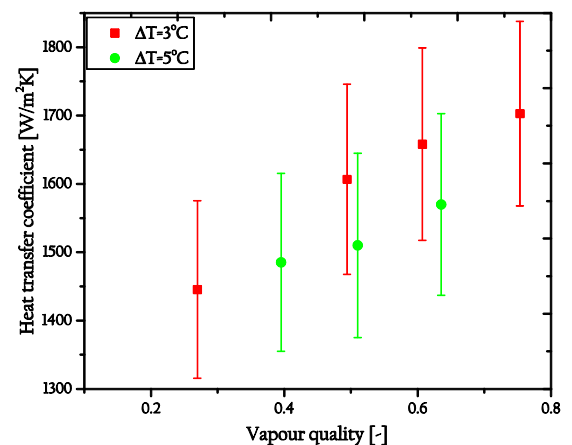

Figure 5. Effect of temperature difference on heat transfer coefficient (G=50 kg/m^{2}s, Horizontal flow)

The heat transfer coefficient is plotted against the mean vapor quality for a mass flux of 50 kg/m^{2}s at different temperature differences in Fig. 5.The significance of the heat transfer coefficient dependence on the ΔT becomes more pronounced whilst there was a negligible dependence on the mean vapour quality. In fact, taking into account uncertainties, the heat transfer coefficient did not show any dependence whatsoever the mean vapour quality but on the temperature difference (ΔT) only

CONCLUSION

Experiments and flow visualization during the condensation at low mass fluxes between 20 – 100 kg/m^{2}s was carried out using R134a refrigerant at mean vapour qualities of between 0.15-0.82 and varying controlled temperature differences inside a smooth horizontal tube was carried out. The experimental data points were plotted on the El-Hajal-Thome flow pattern map. In general, higher heat transfer coefficients were found at lower temperature differences. The higher heat transfer rates were due to the thinning of the liquid layer hence a smaller resistance to heat transfer. The flow pattern was captured, visualized and analysed and found to be mainly stratified and stratified wavy flows. Finally, it was found that as mass flux reduced, more dependence on the temperature difference was noticed.

REFERENCES

[1] N. Kattan, J. R. Thome, and D. Favrat, " Flow boiling in horizontal tubes: Part 1- Development of a diabatic two phase flow pattern," *ASME Journal of Heat Transfer,* vol. 120, pp. 140-147, 1998.

[2] A. Cavallini and R. Zecchin, "A dimensionless correlation for heat transfer in forced convection condensation," in *Proceedings of the Fifth International Heat Transfer Conference*, Tokyo, Japan, 1974, pp. 309-313.

[3] M. K. Dobson and J. C. Chato, "Condensation in smooth horizontal tubes," *ASME Journal of Heat Transfer,* vol. 120, pp. 193-213, 1998.

[4] D. W. Shao and E. Granryd, "Flow pattern, heat transfer and pressure drop in flow condensation; Part I: Pure and azeotropic refrigerants," *HVAC & R Research,* vol. 6, pp. 175-195, 2000.

[5] D. W. Shao and E. Granryd, "Flow pattern, heat transfer and pressure drop in flow condensation; Part II: Zeotropic refrigerants," *HVAC&R Research,* vol. 6, pp. 197-209, 2000.

[6] J. R. Thome, J. El Hajal, and A. Cavallini, "Condensation in horizontal tubes, part 2: New heat transfer model based on flow regimes," *International Journal of Heat and Mass Transfer,* vol. 46, pp. 3365-3387, 2003.

[7] J. R. Thome, "Condensation inside tubes," in *Wolverine Engineering Data Book III*, ed, 2006, pp. 1-27.

[8] C. Aprea, A. Greco, and G. P. Vanoli, "Condensation heat transfer coefficients for R22 and R407C in gravity driven flow regime within a smooth horizontal tube," *International Journal of Refrigeration,* vol. 26, pp. 393-401, 2003.

[9] H.-S. Lee and C.-H. Son, "Condensation heat transfer and pressure drop characteristics of R-290, R-600a, R-134a and R-22 in horizontal tubes," *Heat and Mass Transfer,* vol. 46, pp. 571-584, 2010/05/01 2010.

[10] J. El Hajal, J. R. Thome, and A. Cavallini, "Condensation in horizontal tubes, part 1: Two-phase flow pattern map," *International Journal of Heat and Mass Transfer,* vol. 46, pp. 3349-3363, 2003.

[11] N. Kattan, J. R. Thome, and D. Favrat, "Flow boiling in horizontal tubes: Part 3- Development of a new heat transfer model based on flow pattern," *ASME Journal of Heat Transfer,* vol. 120, pp. 156-165, 1998.

[12] D. Steiner, "Heat transfer to boiling saturated liquids," in *Verein Deutscher Ingenieure (Ed.), VDI-Warmeatlas (VDI Heat Atlas), VDI-Gesellschaft Verfahrenstechnik und Chemieingenieurswesen (GCV)*, ed Düsseldorf, 1993.

[13] T. Nitheanandan and H. M. Soliman, "Analysis of the stratified/nonstratified transition boundary in horizontal and slightly inclined condensing flows," *Canadian Journal of Chemical Engineering,* vol. 72, pp. 26-34, 1994.

[14] H. Soliman, "Correlation of mist-to-annular transition during condensation," *The Canadian Journal of Chemical Engineering,* vol. 61, pp. 178-182, 1983.

[15] H. Soliman, "On the annular-to-wavy flow pattern transition during condensation inside horizontal tubes," *The Canadian Journal of Chemical Engineering,* vol. 60, pp. 475-481, 1982.

[16] E. W. Lemmon, M. L. Huber, and M. O. McLinden, "NIST standard reference database 23: Reference fluid thermodynamic and transport properties (REFPROP), version 9.1, National Institute of Standards and Technology, Standard reference data program, Gaithersburg," 2013.

[17] S. Lips and J. P. Meyer, "Effect of gravity forces on heat transfer and pressure drop during condensation of R134a," *Microgravity Science and Technology,* vol. 24, pp. 157-164, 2012.

[18] S. Lips and J. P. Meyer, "Experimental study of convective condensation in an inclined smooth tube. Part I: Inclination effect on flow pattern and heat transfer coefficient," *International Journal of Heat and Mass Transfer,* vol. 55, pp. 395-404, 2012.

[19] S. Lips and J. P. Meyer, "Experimental study of convective condensation in an inclined smooth tube. Part II: Inclination effect on pressure drops and void fractions," *International Journal of Heat and Mass Transfer,* vol. 55, pp. 405-412, 2012.

[20] S. Lips and J. P. Meyer, "Stratified flow model for convective condensation in an inclined tube," *International Journal of Heat and Fluid Flow,* vol. 36, pp. 83-91, 2012.

[21] R. Suliman, L. Liebenberg, and J. P. Meyer, "Improved flow pattern map for accurate prediction of the heat transfer coefficients during condensation of R-134a in smooth horizontal tubes and within the low-mass flux range," *International Journal of Heat and Mass Transfer,* vol. 52, pp. 5701-5711, 2009.

[22] R. Suliman, M. Kyembe, and J. P. Meyer, "Experimental investigation and validation of heat transfer coefficients during condensation of R-134a at low mass fluxes," presented at the 7th International Conference on Heat Transfer, Fluid Mechanics and Thermodynamics (HEFAT), Antalya, Turkey, 2010.

[23] J. P. Meyer, J. Dirker, and A. O. Adelaja, "Condensation heat transfer in smooth inclined tubes for R134a at different saturation temperatures," *International Journal of Heat and Mass Transfer,* vol. 70, pp. 515-525, 2014.